

Computational Fluid Dynamics Simulation of the Air/Suppressant Flow in an Uncluttered F18 Engine Nacelle

Amalia R. Lopez, Louis A. Gritz, and Basil Hassan

*Sandia National Laboratories
Albuquerque, NM 87185*

Abstract

For the purposes of designing improved Halon-alternative fire suppression strategies for aircraft applications, Computational Fluid Dynamics (CFD) simulations of the air flow, suppressant transport, and air-suppressant mixing within an uncluttered F18 engine nacelle were performed. The release of inert gases from a Solid Propellant Gas Generator (SPGG) was analyzed at two different injection locations in order to understand the effect of injection position on the flow patterns and the mixing of air and suppression agent. An uncluttered engine nacelle was simulated to provide insight into the global flow features as well as to promote comparisons with previous nacelle fire tests and recent water tunnel tests which included little or no clutter. Oxygen concentration levels, fuel/air residence times that would exist if a small fuel *leak* were present, velocity contours, and streamline patterns are presented inside the engine nacelle. The numerical results show the influence of the agent release location on regions of potential flame extinction due to oxygen inerting and high flame strain. The occurrence of inflow through the exhaust ducts on the aft end of the nacelle is also predicted. As expected, the predicted oxygen concentration levels were consistently higher than the measured levels since a fire was not modeled in this analysis. Despite differences in the conditions of these simulations and the experiments, good agreement was obtained between the CFD predictions and the experimental measurements.

Introduction

Fires in aircraft engine nacelles have traditionally been extinguished using Halon 1301 suppression systems. Due to the effectiveness of Halon 1301, reasonable success at suppressing fires under a variety of scenarios has been realized by systems designed with simple design equations. The ban of Halon 1301 production, as a result of a 1994 amendment to the 1987 Montreal Protocol [1], has resulted in numerous investigations of Halon 1301 alternatives with significantly reduced Ozone Depleting Potential (ODP). Despite extensive efforts [2-6], low-ODP agents with the effectiveness of Halon 1301 have not been discovered. A logical progression from the quest for such “drop-in” replacement systems is to employ alternate emerging fire suppression techniques (such as the use of gas generators alone or in conjunction with chemical suppressants) in optimized suppression systems. Optimized suppression, as opposed to the use of a suppressant (such as Halon 1301) that is capable of very effective chemical inerting at low concentrations, requires additional insight into the essential features of nacelle fires.

The ability to develop the tools needed to realize significant progress in the nacelle fire problem is expected to rely on the ability for the “first order effects,” including the coupling of these effects,

to be understood via an integrated experimental and numerical investigation. Among the “first order effects” identified as a result of previous fire physics studies [7] is the mixing of fuel and air. The mixing of fuel with a primary air flow is a function of the nature of the fuel release and is therefore highly scenario-specific. **The** essential and salient features of the primary air flow, and the transport of suppressant from a solid propellant gas generator (SPGG) released in a design-specified manner, are largely independent of the fire scenario and therefore form the foundation for the design and assessment of alternative suppression system effectiveness.

Computational Fluid Dynamics (CFD) simulations of the air and suppressant flow within an uncluttered F18 engine nacelle have been performed to provide insight into the global flow features. The uncluttered geometry ensures the tractability of the simulations and promotes comparison with previous nacelle fire tests [8] and recently performed water tunnel tests [9] which included little or no clutter. Two different injection locations of suppressant were analyzed to understand the effect of injection position on the global flow patterns and the mixing of air and suppression agent. The present simulation did not include a fire inside the engine nacelle; however, a recent numerical simulation [10] was performed of a fire in the same F18 engine nacelle geometry using the VULCAN [11] fire field model. **As** expected, the fire field model results showed that the presence of a flame zone had very little impact on the velocity field.

The present work will describe the general features of the flow field inside an uncluttered F18 engine nacelle. Oxygen concentration levels, fuel/air residence time that would exist if a small fuel *leak* were present, velocity contours, and streamline patterns are predicted inside the engine nacelle for two suppressant injector locations. Despite slightly different conditions, experimental measurements of oxygen concentration are compared with the CFD predictions. Overall, good agreement was obtained between the CFD predictions and the experimental measurements.

Based on the literature search performed to date, these calculations represent the first numerical simulations of the air/suppressant flow in an actual nacelle geometry. Previous CFD calculations, including suppressant transport, in a smooth annular geometry [12] have met with limited success as exhibited by poor agreement between predicted and experimentally-measured concentrations.

Gas Dynamics Modeling

The turbulent mixing of the air and suppressant (without fire) was modeled using the CFD-ACE [13,14] commercial code. CFD-ACE is a pressure-based code that solves the Favre-averaged Navier-Stokes equations. These equations model the conservation of mass, momentum, and energy for unsteady, compressible turbulent flows. The governing equations are solved sequentially in an implicit, iterative manner using a finite volume formulation. Various options for modeling turbulence, reaction chemistry, and multi-phase flows are available. In the present calculations, the governing equations are solved until a steady-state solution is reached. The k- ϵ turbulence model of Launder and Spalding [15] is used.

Engine Nacelle Geometry and Grid Generation

Figure 1 shows the uncluttered engine nacelle geometry used in the present simulations. The geometry was based on the full-scale engine nacelle simulator at the Aircraft Survivability Branch

of the Naval **Air** Warfare Center, Weapons Division at China Lake, California, but does not include the nacelle ribs or any of the clutter between the engine and the nacelle. The computational model was constructed from an Autocad representation of the F18 nacelle ribs which was used to construct a 1/6 scale model of the uncluttered nacelle for the water tunnel tests. The air inlet scoop is located circumferentially 154degrees clockwise from the vertical axis and positioned at an angle of 20 degrees above the longitudinal axis as noted in Figure 1.

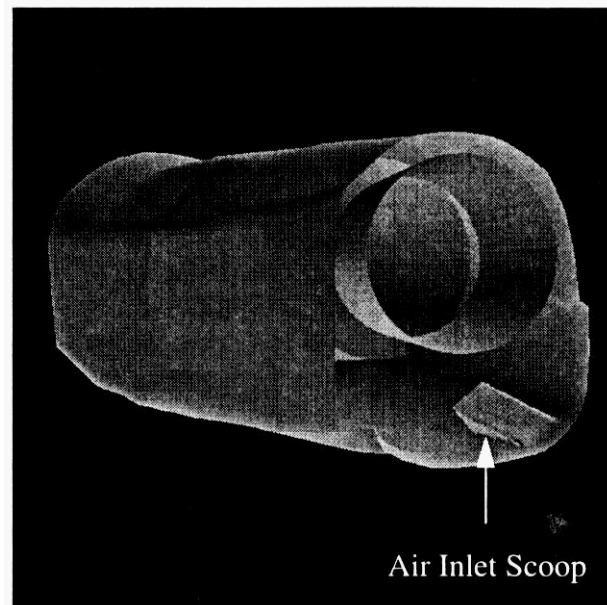


Figure 1: Solid model of uncluttered F18 engine nacelle.

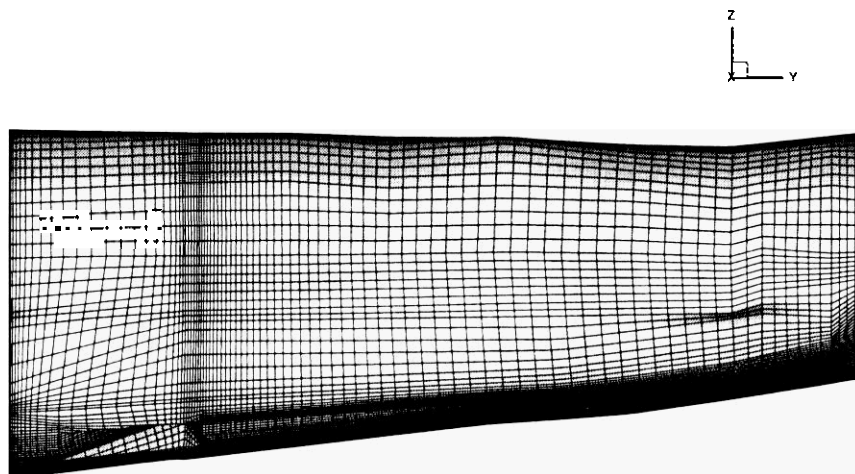


Figure 2: Computational grid overlaid on F18 nacelle surface.

Figure 2 shows a side view of the nacelle with the computational grid overlaid on the surface. GRIDGEN [16] Version II was used to generate the structured, computational grid. The grid was

created in three main sections: the suppressant injector/air inlet section; the middle section between the air inlet and the exhaust ducts; and the exit section up to the end of the nacelle. Part of the air inlet scoop can be seen in the lower left side of this figure. The grid was highly refined near the suppressant injector locations and near the air scoop. Three-dimensional calculations were performed using 88 axial by 24 radial by 105 circumferential (a total of 221,760) grid points.

Boundary Conditions

The flow conditions addressed in the simulations are shown in Table 1 and were based on a specific series of tests performed at China Lake [8]. The velocity of the air entering the nacelle was determined from a specified mass flow rate of 0.953 kg/s (2.1 lbm/s) and the area of the inlet. The air flow within the inlet scoop was not modeled. Since this flow is expected to be fully turbulent, a uniform velocity profile directed at an angle of 15 degrees above the air scoop (to account for a scoop geometry which includes an open region on the top surface of the scoop) was specified at the inlet boundary of the nacelle domain. The exhaust ducts were modeled using two rectangular-shaped, constant pressure regions at the top and bottom of the aft end of the nacelle. Sea level pressure and temperature values were assumed at the air inlet as well as at the exhaust ducts.

	Suppressant Inlet	Air Inlet	Exhaust Outlets
Mass Flow Rate (kg/s)	0.340 (0.75 lbm/s)	0.953 (2.1 lbm/s)	
Velocity (m/s)	486 (1595 ft/s)	57 (187 ft/s)	
Temperature (K)	672 (750° F)	300 (80° F)	300
Pressure (KPa)	629 (91 psi)	101 (14.7 psi)	101

Table 1: Flow conditions specified at engine nacelle inlets and outlets.

The suppression agent in this study is generated by the combustion of solid propellant in an SPGG. The suppressant consists of 55% CO₂, 28% N₂, and 17% H₂O vapor. At the suppressant inlet in the nacelle, compressible gas dynamic relations [17] predict that the propellant flow from the gas generator chokes at the exit of the feeder tube producing a supersonic flow into the nacelle. Given a measured static temperature of 672 K (750 °F) at the suppression inlet, it can be shown using compressible gas relations that the static pressure is 629 KPa (91 psi). A uniform velocity profile was assumed at the suppressant inlet based on the mass flow rate of suppressant and the area of the feeder tube.

In turbulent mixing calculations, the mass transport coefficients used in the Navier Stokes equations are determined from the turbulent Schmidt number. From several different sources [18,19] it was concluded that the Reynolds analogy which states that the heat and momentum transfer coefficients are the same also holds for the mass transfer coefficients for gases. Thus, both the turbulent Prandtl number and Schmidt number are near unity. In order to validate the computer code, a propane jet in co-flowing air stream simulation was run in order to compare mixture fractions with experimental measurements. The predicted propane mixture fractions agreed very

well with the experimental data using a turbulent Schmidt number of 0.9 and a turbulent Prandtl number of 0.9. These same values were therefore used in this study.

Computational Requirements

The computational simulations were performed until convergence consisting of a 2-3 order of magnitude reduction in all residuals over the computational domain was achieved. Typically, 3000 iterations are required to obtain 4-5 orders of magnitude reduction in the residuals; however, in the present simulations, the residuals leveled off due to oscillations in the solution around the suppressant injector. This behavior is a result of a computational grid which is too coarse to fully resolve the flow within the feeder tube, and therefore immediately adjacent to the suppressant injector. In fact, the minimum cell size, and hence the size of the overall grid, was dictated by the small size of the injectors, which are each 1.6 **cm** (*5/8 in*) in diameter. Therefore, a trade off between the total number of grid points and the time and memory required to get a solution was necessary. The solution required 3.0 *msec/cell/iteration* of CPU time and 212 *Mbytes* of RAM on a Sun Microsystems SPARCstation 10 Model **HS** 125 workstation. These 3000 iterations required a total CPU time of 500 hours.

Results

Numerical simulations of the air-suppressant flow inside the nacelle for two different suppressant injection locations were conducted. The first injection location (inboard) was chosen to be the same as the original Halon injection location. The second injection location (outboard) was chosen to correspond to a new location which demonstrated improved ability to extinguish fires resulting from fuel leaks on the outboard side of the nacelle in fire suppression tests conducted at China Lake. Improved system performance is expected with the new injection location since the suppressant is introduced into the nacelle where it can readily mix with the incoming air which is required to sustain a fire.

Inboard Injector Location

Figure 3 shows the predicted air isosurface and the suppressant streamline pattern. In this figure, the geometry has been rotated 180° from Figure 1 for a better view of the air and suppressant inlets. The air isosurface shows the air flow (*i.e.* 0.90) from the inlet to the engine. After the air stream impacts the engine, it spreads circumferentially in both directions around the engine. In addition, there is a smaller air isosurface near the aft end of the nacelle which is the result of air flow into the nacelle through the exhaust ducts. The streamline pattern shows the suppressant jet flow inside the nacelle. The streamlines are colored by the air mass fraction such that the darkest contour (*i.e.* 0.0) corresponds to pure suppressant. It can be seen that the suppressant quickly mixes with the air such that the streamlines become lighter. This figure also shows the high velocity jet flow from the injector to the end of the nacelle. At the end of the nacelle, the suppressant-air jet splits and starts to flow circumferentially around the engine in both directions.

Figure 4 shows another view of the isosurface/streamline pattern. The streamlines show that after the suppressant-air mixture wraps around the engine, it flows back upstream towards the nacelle bulkhead. Near the front of the nacelle, the streamlines start to wrap around the engine on the inboard side. From Figure 3, the streamlines show that the mixture continues to wrap around the

engine and then turns to flow forward again between the main suppressant stream and the engine. Near the aft end of the nacelle, the streamlines reverse direction again and the mixture continues to flow around the air inlet forming a large recirculation pattern within the nacelle.

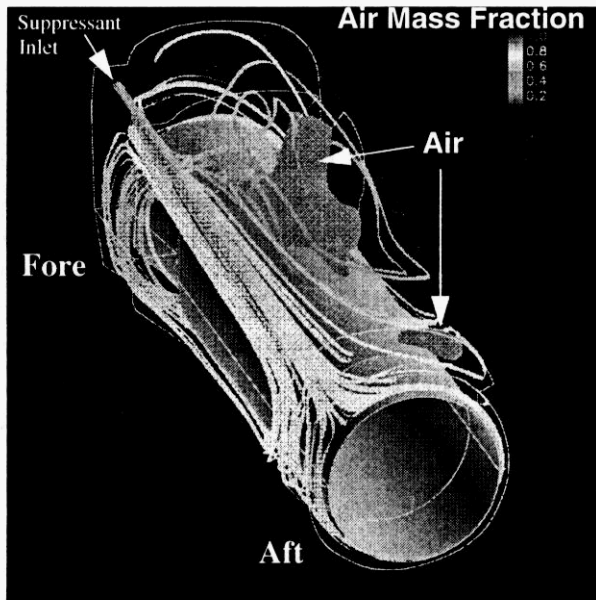


Figure 3: Air isosurface and suppressant streamline pattern for inboard injector.

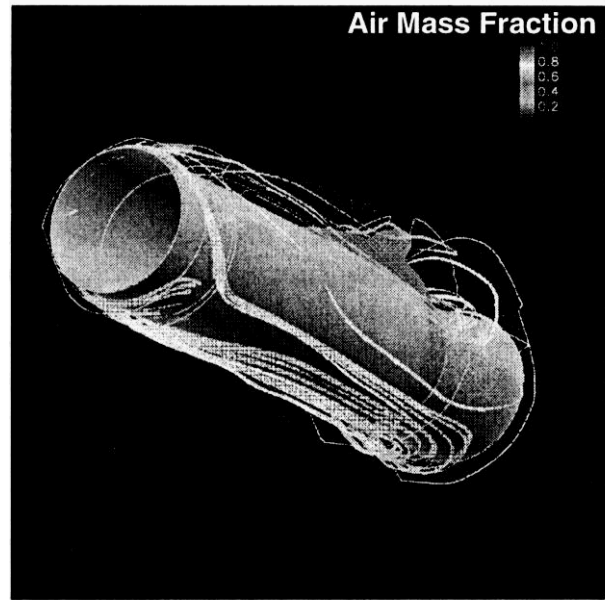


Figure 4: Air isosurface and suppressant streamline pattern for inboard injector.

(Views rotated 180° for clarity).

Figure 5 shows the axial velocity contours at a location **48 cm (19 in)** on the fore side of the air inlet. This figure shows the high velocity flow of suppressant in the lower inboard side of the nacelle. In addition, this figure shows a very large region of negative axial velocity which is caused by the flow that has reached the end of the nacelle and is now moving back towards the nacelle bulkhead.

Figure 6 shows two isosurfaces with different air mass fractions. As before, the geometry has been rotated 180° from Figure 1 for a better perspective of the air and suppressant inlets. The air isosurface again shows the air flow from the inlet to the engine, while the other isosurface corresponds to a mixture of 0.65 air and 0.35 suppressant. A mass fraction of 0.65 air corresponds to a mass fraction of 0.15 oxygen. These levels were selected for presentation based on published lower flammability limits (*i.e.* minimum oxygen requirements for combustion) for heavy hydrocarbon fuels [20] of 0.1345 mole fraction which corresponds to 0.15 mass fraction of oxygen. The 0.65 air isosurface therefore shows the inerted region in which the concentration of oxygen is too low to sustain a fire. For the given mass flow rate of suppressant and air, a perfect, uniform mixture of the gases results in a mass fraction of 0.74 air and 0.17 oxygen. Thus, as mentioned in the description of the nacelle fire tests at China Lake [8], insufficient agent is released under these conditions for complete inerting. A perfect mixture of suppressant and air is therefore not desirable with this agent release level since it produces an oxygen level which is within the flammability regime throughout the entire region of interest.

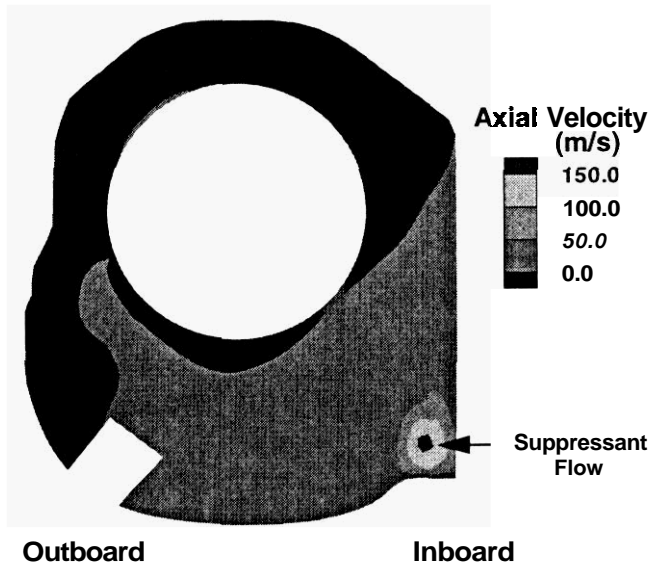


Figure 5: Axial velocities in a cross section at the tip of air scoop for inboard injector.

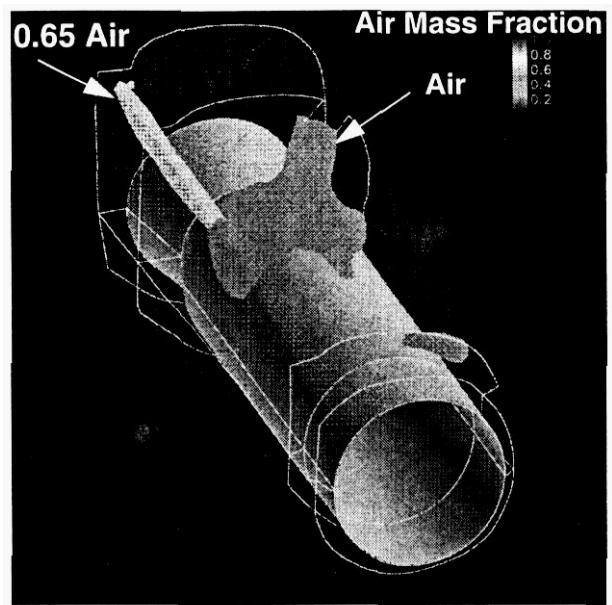


Figure 6: Air and suppressant isosurfaces at both inlet locations for inboard injector (View rotated 180° for clarity).

Despite differences in the level of clutter present in the full scale simulator and the geometry used for these calculations, and the presence of a fire in the tests, predicted oxygen concentrations *are* compared with data [21] acquired during the tests at China Lake. Additional uncertainty regarding the exact location of the measurement positions, specifically in regions of high gradients, is also expected to affect the agreement between model results and the measured concentrations. The purpose of these comparisons is to assess the potential for differences in the overall trends evident in the two sets of results. Figures 7-9 show contour plots of oxygen concentrations at three different axial locations which correspond to the position of measurements performed in the China Lake test. Position #1 is approximately 31.5 cm (12.4 in) fore of the air inlet on the outboard side, Positions #2 and #5 are both approximately 10 cm (4in) aft of the air inlet on the outboard side, and Position #3 is located approximately 83 cm (32.8 in) aft of the air inlet on the inboard side. It should be noted that all figures show the mass fraction of oxygen and not volume (or mole) fraction.

Figure 7 shows contours of oxygen concentration ranging from the flammability limit (*i.e.* 0.15) to pure air (*i.e.* 0.23) at the axial location corresponding to Position #1. The darkest contour, which corresponds to an oxygen mass fraction of 0.15 and below, shows the region where a fire would be extinguished due to insufficient oxygen. In this figure, the darkest region is in the lower right corner in the vicinity of the injector. The maximum oxygen concentration shown in this figure is around 0.20. Since this axial location is on the fore side of the air inlet, the oxygen concentrations are below that for pure air due to the recirculation of suppressant into this region. In the China Lake test, a 15% volume fraction of oxygen at the 9:00 o'clock position was obtained at a time corresponding to the end of the agent release (*i.e.* 5 sec). This volume fraction corresponds to an oxygen concentration level of 16.5% based on mass fraction. In this same region, the predicted

oxygen mass fractions are approximately 17.5% which shows reasonable agreement with the measurements. As mentioned previously, differences between the predictions and measurements were expected since the nacelle geometry used in the tests included some clutter and ribs. In addition, the China Lake tests included a fire which would tend to deplete the oxygen concentration levels.

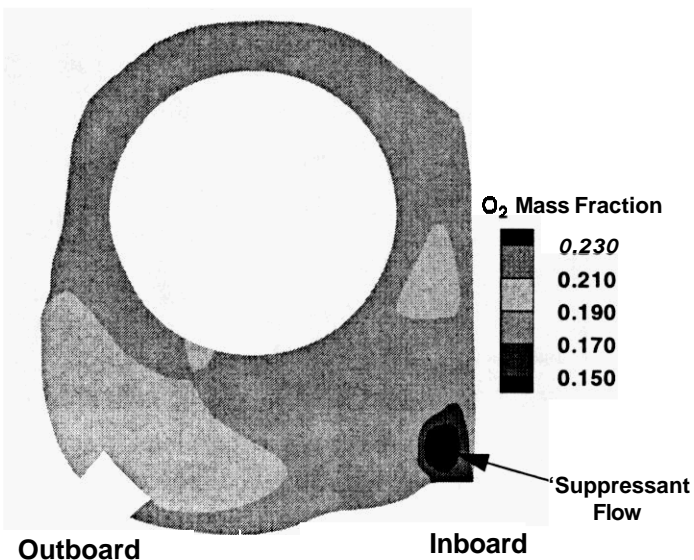


Figure 7: Oxygen concentrations in a cross section at Position #1 for inboard injector.

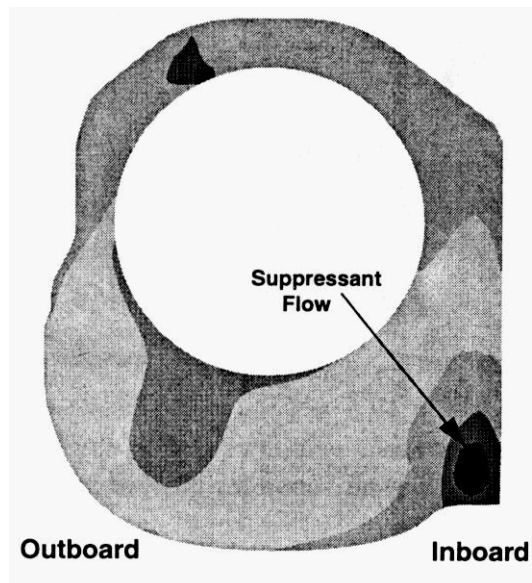


Figure 8: Oxygen concentration in a cross section at Position #2 & #5 for inboard injector.

Figure 8 shows contours of oxygen concentration at Positions #2 and #5. Again, the region below the 0.15 oxygen concentration is limited to the neighborhood of the injection position. In this figure, the effect of the air inlet is shown by the contour on the lower left side of the cross section that extends to the engine. Also, a small dark region indicating low oxygen concentration can be observed in the top left side of the cross section. The presence of this region shows that the suppressant has been carried to the top of the nacelle by the flow which has wrapped around the engine and is now moving from the aft end of the nacelle towards the bulkhead as shown by the streamline pattern in Figure 4. In the China Lake test, a 18.5% volume fraction of oxygen (20.4% based on mass fraction) was measured at a position in the main air flow for Position #5 and just above the main air for Position #2. In this same region, the predicted oxygen concentration is about 22% and again shows fair agreement with the measurements. This value is close to pure air since it is located in the main air stream.

Contours of oxygen concentration at Position #3 are shown in Figure 9. At this axial location, only a small region is observed where the oxygen concentration is below the flammability limit. In addition, the region of high oxygen concentration has been significantly reduced. Oxygen volume fractions of 16.5% (18.2% mass fraction) were measured in this region at the 3:00 o'clock position during the China Lake test. In keeping with the general trends of the data, oxygen concentrations of about 19.2% were predicted.

Overall, Figures 7-9 indicate that there is a very small region where the fire will be extinguished on the basis of the oxygen concentration flammability limit. Another important factor which determines whether a fire is extinguished in a fuel-air mixture is the strain rate as indicated by the residence time of the fuel and air streams. Areas of small residence time are indicative of high flame strain rate zones where fires cannot survive. Based on Magnussen's Eddy Dissipation Concept Combustion Model [22], it can be shown that the residence time in the combusting regions of the fine turbulent structures is a function of the kinematic viscosity divided by the turbulent kinetic energy dissipation rate. When this residence time is less than the chemical time scales for combustion (on the order of 7.0×10^{-5} seconds for an air/methane mixture), the fire will be extinguished due to excessive flame strain. This concept forms the basis for a suppression model that is presently being developed for fire field models [23].

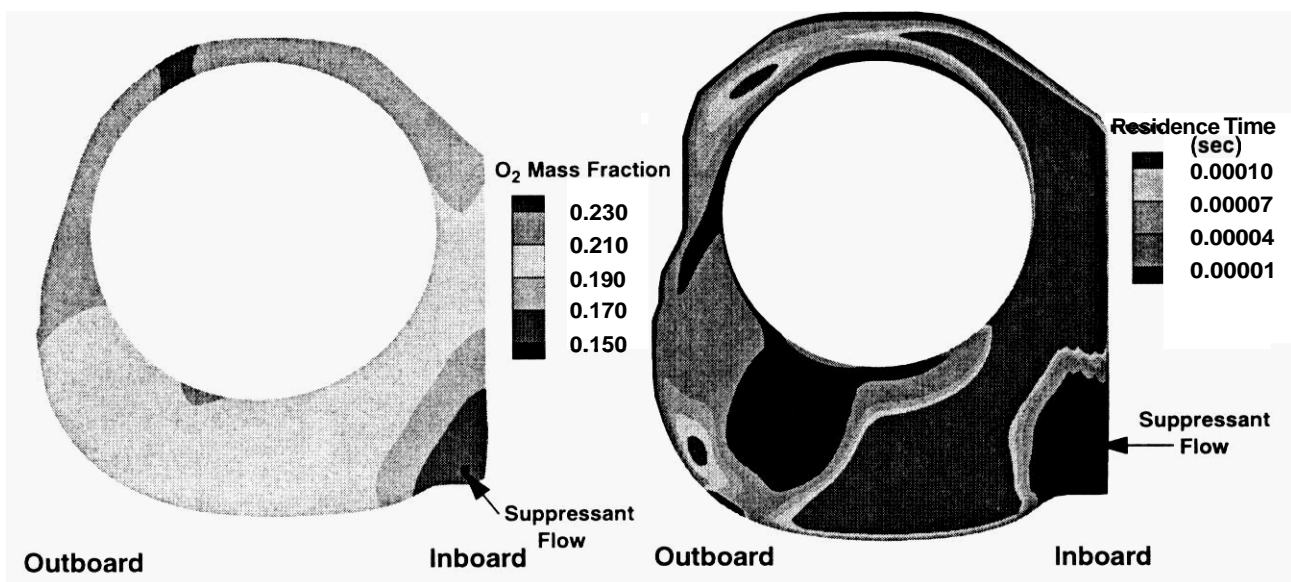


Figure 9: Oxygen concentrations in a cross section at Positions #3 for inboard injector.

Figure 10: Residence times in a cross section 10 cm (4 in) on the aft side of the air inlet for inboard injector.

Figure 10 shows contours of the residence time at an axial location that is 10 cm (4 in) beyond the air inlet. This location was based on the location of the fuel release and subsequent fire in the previously-referenced China Lake tests [21]. The results show high residence times on the inboard side of the nacelle except in the lower inboard corner where the high speed flow of suppressant exists. Thus, the flow above the suppressant stream must experience a low turbulent strain rate. In addition, high residence times occur along the bottom of the nacelle where large recirculation regions exist except in the lower outboard side of the engine nacelle where the high speed air flow from the inlet reduces the residence times. Thus, residence times tend to be high except in the air and suppressant flow regions. Provided that there is a sufficient flow of inlet air to maintain burning in these regions of high residence times (both from an oxygen starvation and a suppressant inerting perspective), a fire will persist in these regions.

Therefore, it is important to also consider residence time when determining the survivability of a fire. For example, based on the oxygen concentrations shown in Figure 8, a fire will survive at all locations except in the region of the suppressant flow. However, Figure 10, which is at the same axial location as Figure 8, shows a large region on the outboard side of the nacelle where the residence times are below those needed to sustain burning. Lowest residence times are observed in the region where the oxygen concentration are the highest. Therefore, a combination of these two measures may provide the best indicator of suppression system performance.

Outboard Injector Location

Calculations of air and suppressant flow were also performed for the case where the agent is injected from the lower portion of the bulkhead on the same (outboard) side as the air inlet. Experimental results show that this location provides a significant improvement in the ability to extinguish fires resulting from a fuel leak on the outboard side of the nacelle. General improvements in extinguishing ability can also be expected given this modification since sustained burning is only likely in areas where oxygen requirements are satisfied by inlet air flow. Due to limited circulation of the inlet air, fires formed in other regions are likely to rapidly exhaust the available oxygen.

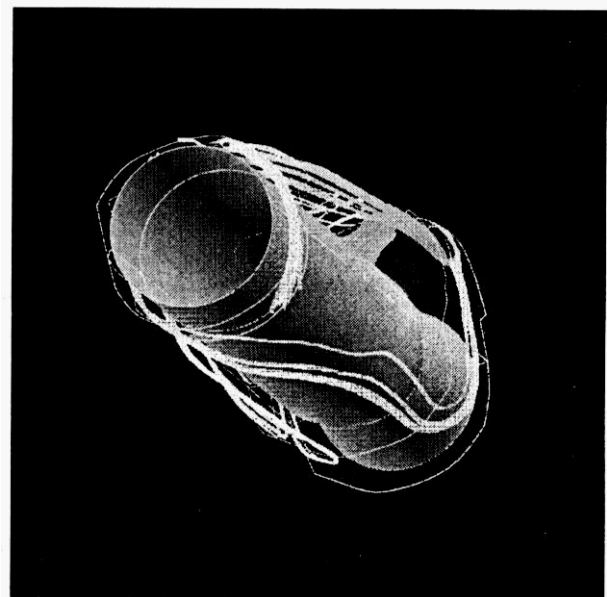
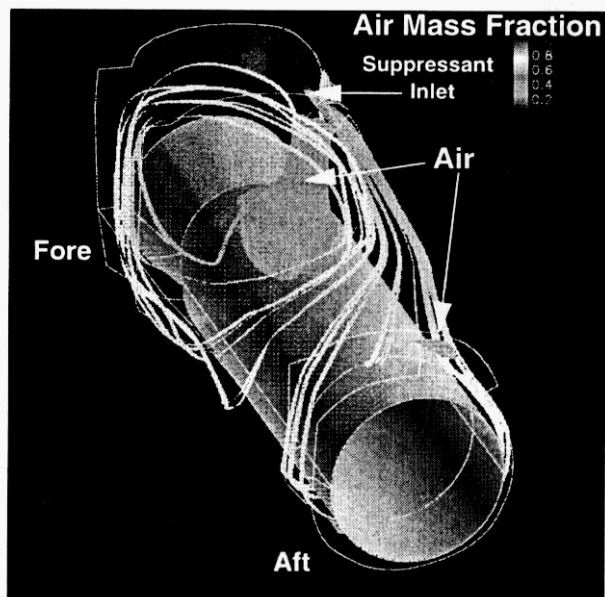


Figure 11: Air isosurface and suppressant streamline pattern for outboard injector.

(View rotated 180° for clarity).

Figure 12: Air isosurface and suppressant streamline pattern for outboard injector.

Figure 11 shows the predicted air isosurface and the suppressant streamline pattern. In this figure, the geometry has again been rotated 180° from Figure 1 to provide a better view of the air and suppressant inlets. The boundary of the air flow from the inlet scoop is represented by the air isosurface (*i.e.* 0.9). After the air stream impacts the engine, it spreads circumferentially in the counterclockwise direction around the engine. In addition, there is a smaller air isosurface near the aft end of the nacelle which is the result of air flow into the nacelle through the exhaust ducts. The

streamline pattern shows the suppressant jet flow inside the nacelle. The streamlines are colored by the air mass fraction such that the darkest contour (*i.e.* 0.0) corresponds to pure suppressant. Again, it can be seen that the suppressant quickly mixes with the air such that the streamlines become lighter. This figure also shows a high velocity suppressant jet flow from the injector to the aft end of the nacelle. At the aft end of the nacelle, the suppressant-air stream splits and **starts** to flow circumferentially around the engine in both directions.

Another view of the isosurface/streamline pattern is given in Figure 12. The streamlines show that after the suppressant-air mixture wraps around the engine, it flows back upstream towards the nacelle bulkhead. Near the fore end of the nacelle, the streamlines wrap around the engine on the outboard side between the main suppressant stream from the inlet and the nacelle. From Figure 11, the streamlines show that the mixture turns to flow forward towards the inboard side of the nacelle. Near the aft end of the nacelle, the streamlines reverse direction again and the mixture continues to flow around the air inlet forming a large recirculation region.

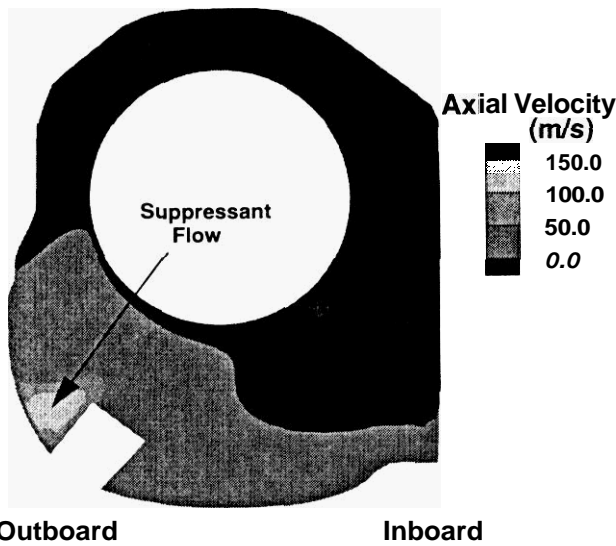


Figure 13: Axial velocities in a cross section at the tip of air scoop for outboard injector.

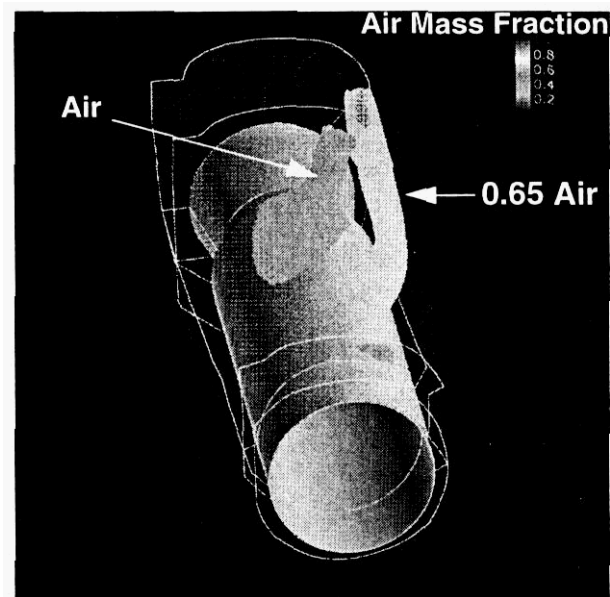


Figure 14: Air and suppressant isosurfaces at both inlet locations for outboard injector (View rotated 180° for clarity).

Figure 13 shows the axial velocity contours at a cross section near the tip of the air scoop. The high velocity flow of suppressant in the lower outboard side of the nacelle is noted in this figure. In addition, this figure shows a very large region of negative axial velocity which is a result of the flow that has reached the aft end of the nacelle and is now flowing back towards the nacelle bulkhead.

Significant alterations in the air flow are therefore observed when the suppressant injector position is relocated to the outboard side. Recall in Figure 3 that the inlet air stream (as shown by the air isosurface) spreads around the engine in both directions when the agent was released from the

inboard injector. However, for the outboard injector, Figure 11 shows that the air stream only spreads towards the inboard side and away from the suppressant flow which appears to deflect the incoming air stream. In addition, the outboard injector streamlines curve towards the inboard side as the suppressant flows from the injector to the aft end of the nacelle; whereas, the inboard injector streamlines show the main suppressant jet flowing in a straight line from the injector to the aft end of the nacelle. Also, the location of the negative velocity contours for the outboard injector are mirror images of the contours obtained when the agent was released from the inboard injector. This trend is to be expected because the injectors are located in mirror image positions and the reverse flow (*i.e.* the flow which reaches the aft end and flows back towards the bulkhead) always occurs on the side opposite to the main suppressant jet.

Figure 14 shows two isosurfaces with different air mass fractions. The geometry was rotated, as before, 180° to provide a better view of the air and suppressant inlets. The air flow from the inlet is represented by the air isosurface, while the other isosurface represents an inert mixture of 0.65 air and 0.35 suppressant which is sufficient to reduce the oxygen concentration below the necessary concentration to sustain a fire. This region extends much farther from the bulkhead with the outboard injector.

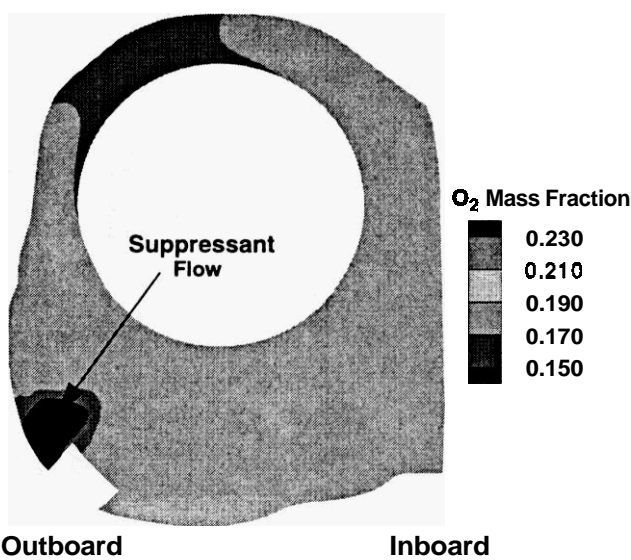


Figure 15: Oxygen concentrations in a cross section at Position #1 for outboard injector.

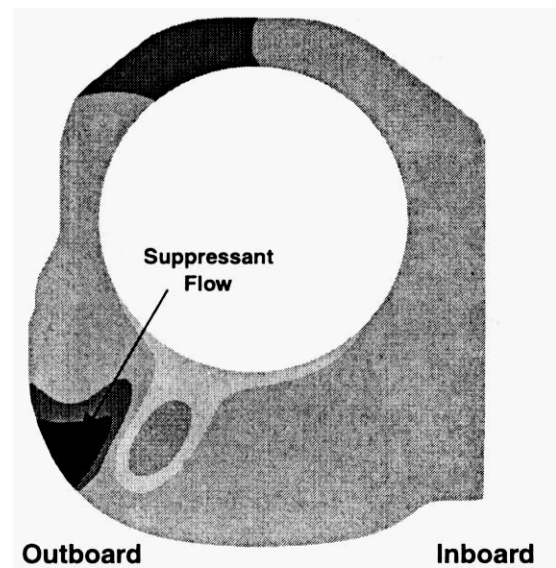


Figure 16: Oxygen concentrations in a cross section at Position #2 & #5 for outboard injector.

Contours of oxygen concentration ranging from the flammability limit (*i.e.* 0.15) to pure air (*i.e.* 0.23) are shown in Figure 15 for a cross section at the axial location of Position #1. Position #1 is about 31.5 cm (12.4 in) on the fore side of the air inlet on the outboard side. The darkest contour, which corresponds to an oxygen mass fraction of 0.15 and below, shows the region where a fire would be extinguished due to insufficient oxygen. As expected, the region of lowest oxygen concentration is located in the lower left corner near the injector as shown by the darkest region in Figure 15. Also, a low oxygen concentration (dark) region is observed in the top left side of the cross section. This trend is a result of the presence of suppressant which has been advected to the

top of the nacelle by the flow which wrapped around the engine near the aft end and is now moving from the aft to the fore end of the nacelle. The maximum oxygen concentration shown in this figure is around 0.20. Since this cross section is between the air inlet and the bulkhead, the reduction in the oxygen concentration observed in these results is a consequence of suppressant which is recirculating as shown by the streamlines in Figures 11 and 12. In the China Lake test which corresponds to the conditions represented in this simulation [21], a 14% by volume (15.4% based on mass fraction) oxygen concentration level was measured at the end of the agent release. The measurement was taken at approximately the 9:00 o'clock position. In this same region, a slightly higher oxygen concentration of about 17.5% is observed in the computational results. As mentioned previously, differences between the predictions and measurements were expected since the nacelle geometry used in the tests included some clutter and ribs. In addition, the China Lake tests included a fire which would tend to reduce the overall oxygen concentration levels.

Figure 16 shows contours of oxygen concentration at axial locations corresponding to Positions #2 and #5. Positions #2 and #5 are both about 10 *cm* (4 *in*) on the aft side of the air inlet on the outboard side. Again, the region below the 0.15 oxygen concentration is limited to the injection location. In this figure, the flow from the air inlet is shown by the oval concentration contour on the lower left side of the cross section. Oxygen concentration data from China Lake tests include a volume fraction of 15.5% oxygen (17.1% by mass) and 13% oxygen (14.3% by mass) at Positions #5 and #2, respectively. The measurements were taken in the main air flow for Position #5 and just above the main air for Position #2. In this same region, the predicted oxygen concentration is about 21.5% at Position #5 and 19.5% at Position #2. Agreement at these locations are subject to uncertainty in the actual radial and circumferential positions of the measurement locations. Figure 16 shows that a slight upward shift in location would cause a significant reduction in the oxygen concentrations.

Figure 17 shows contours of oxygen concentration at Position #3. Position #3 is about 83 *cm* (32.8 *in*) aft of the air inlet on the inboard side. At this axial location, the region where the oxygen concentration is below the flammability limit still exists. Measured oxygen concentrations by volume, of 15.5% (17.1% based on mass fraction) taken at approximately the 3:00 o'clock position in this cross section, agree reasonably well with the predicted oxygen concentration of 18.1%.

It is clear that relocating the injector position to the outboard side of the nacelle has a pronounced effect on the oxygen concentrations in the nacelle. The numerical predictions show that this change results in a reduction in oxygen concentrations around the air inlet as well as further downstream. Also, the low oxygen (dark) region that exists along the top outboard side of the nacelle developed sooner and was larger with the outboard injector. These differences can also be observed in the experimental data which show approximately equal oxygen concentrations at Positions #2 and #5 for the inboard injector because the suppressant is on the opposite side. When the injector is located on the outboard side, and the agent is injected on the same side as the air inlet, lower oxygen concentrations are observed at Position #2 (which is above the main air stream) than Position #5 which is in the main air stream.

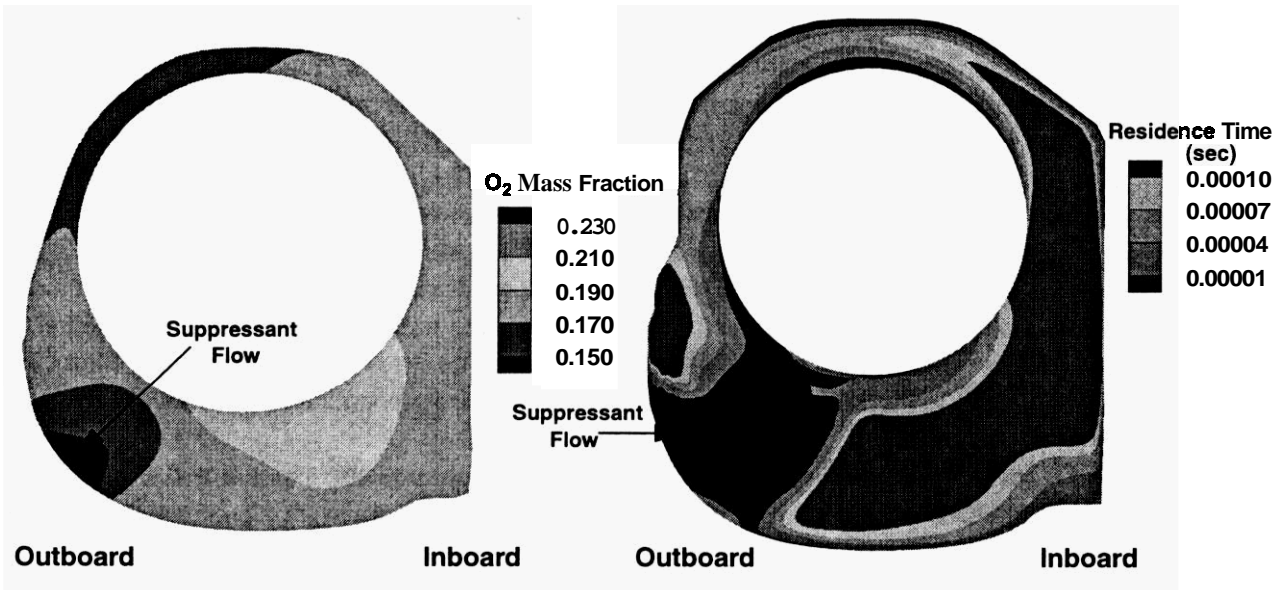


Figure 17: Oxygen concentrations in a cross section at Position #3 for outboard injector.

Figure 18: Residence times in a cross section 10cm (4 in) on the aft side of the air inlet for outboard injector.

Overall, Figures 15-17 again indicate that there is a very small region where the fire will extinguish based on the oxygen concentration flammability limit. Residence time of fuel/air mixtures that may be present in the nacelle during a fire scenario are therefore again investigated as an additional means of assessing system performance.

Figure 18 shows contours of the residence time at an axial location 10cm (4 in) aft of the air inlet. High residence times, which correspond to low turbulent strain rates and therefore stable combustion, occur on the inboard side of the nacelle where lower velocity flows are observed. In addition, high residence times occur along the bottom of the nacelle where large recirculation regions exist. However, in the vicinity of the high speed air and suppressant streams, residence times are reduced on the lower outboard side of the engine nacelle. Thus, residence times tend to be high except near the air and suppressant flow regions.

Overall, the residence times resulting from agent released at the outboard injector location are very similar to the inboard injector results. The location of the injectors produces significant differences in the region of low residence times. In addition, the outboard injector produces a region of high residence times on the outboard side near the middle of the nacelle. This region, which could be capable of supporting a stabilized flame is characterized by a small recirculation region that develops just above the suppressant stream.

The results obtained for the case where the agent is released in the outboard location emphasize the variation in potential fuel/air residence times that occurs as a consequence of changes in the system design. Since fuel/air residence time appears to provide a secondary means of assessing regions of fire suppression in the nacelle environment, combined consideration of agent inerting and agent release-induced turbulent flame strain (as represented by residence time) appears to be a promising

approach for optimized suppression system design. This conclusion is supported by the results presented here where the lowest residence times shown in Figure 18 occurred in the region where the oxygen concentration was the highest as shown in Figure 16.

Conclusions

Computational Fluid Dynamics (CFD) results of the air and suppressant flow within an uncluttered F18 engine nacelle were presented. Two different injection locations of suppressant were analyzed in order to understand the effect of injection position on the global flow patterns and the mixing of air and suppression agent. Numerical results of oxygen concentration levels, the flow residence times, velocity contours, and streamline patterns were discussed to illustrate features of the complex three-dimensional flow. The results show a flow structure which is heavily influenced by the injection of the suppressant. Flow which is primarily fore to aft at the bottom of the nacelle (near the air and suppressant inlets) reverses at the aft end of the nacelle and flows from aft to fore along the top of the nacelle before moving down along the bulkhead and mixing with the incoming flow. This complex flow structure also includes local recirculation regions, and regions of comparatively quiescent flow. In addition, the occurrence of inflow through the exhaust ducts on the aft end of the nacelle was also predicted.

The numerical results show the influence of two different agent release locations on regions of potential flame extinction due to oxygen inerting and high flame strain. Significant differences between the flow resulting from suppressant injection on the inboard and outboard sides were observed. Inboard and outboard regions of flow from fore to aft and flows from aft to fore were interchanged as a result of relocating the suppressant injector. Overall, the numerical predictions show better mixing of the suppressant and air streams when the injector is located on the outboard side. This new location produces lower oxygen concentrations around the air inlet as well as further downstream. As expected due to presence of the fire in the experiments, the predicted oxygen concentration levels were consistently higher than the measured levels. Despite differences in the conditions of these simulations and the tests at China Lake, good agreement to within 2-3% between the two sets of results was obtained.

Another important factor which determines whether a fire is extinguished in a fuel air mixture is the strain rate as indicated by the residence time of the fuel and air streams. In the present study, the lowest residence times occurred in the region where the oxygen concentration was the highest. Therefore, a combination of these two measures may provide the best indicator of suppression system performance.

Overall, the numerical results presented in this paper provide insight into the complex three-dimensional flow fields that occur in aircraft engine nacelles, and indicate the utility of such modeling efforts for future investigations of nacelle fire suppression.

Acknowledgments

The authors wish to thank Leo Budd, Mark Swett and Deborah Paull from the Naval Air Warfare Center, Weapons Division and Knox Millsaps from the Naval Post Graduate School for their continued assistance and consultation on the F18 geometry and flow conditions. Also, the authors wish to thank Robert Cochran and William Oberkampf of Sandia National Laboratories for their assistance with the numerical modeling.

This work was supported by the United States Department of Defense, Naval Air Warfare Center, Weapons Division, Aircraft Survivability Branch and the Engineering Sciences Research Foundation at Sandia National Laboratories. Sandia is a multiprogram laboratory operated by Sandia Corporation, a Lockheed Martin Company, for the United States Department of Energy under contract DE-AC04-94AL85000.

References

- [1] Harrington, J.L., *NFPA Journal*, pp. 38-42, March/April, 1993.
- [2] Pitts, W., Nyden, M., Gann, R., Mallard, W., and Tsang, W., "Construction of an Exploratory List of Chemicals to Initiate the Search for Halon Alternatives," NIST TN 1279, National Institute of Standards and Technology, Gaithersburg, MD, 1990.
- [3] Zallen, D.M., "Halon Replacement Study," SBIR Report ZIA-92-001 Aeronautical Systems Division, Wright-Patterson **AFB**, Zallen International Associates, Albuquerque, NM, February 28, 1992.
- [4] Grosshandler, W., Gann, R., and Pitts, W., eds., "Evaluation of Alternative In-Flight Fire Suppressants for Full-scale Simulated Aircraft Engine Nacelles and Dry Bays," NIST SP 861, National Institute of Standards and Technology, Gaithersburg, MD, 1994.
- [5] Miziolek, A., and Tsang, W., eds., "Halon Replacements: Technology and Science," ACS Symposium Series No. 611, American Chemical Society, Washington, D.C., 1995.
- [6] Gann, R.G., ed., "Fire Suppression System Performance of Alternative Agents in Aircraft Engine and Dry Bay Laboratory Simulations," NIST Special Publication 890, Vol. I and II, National Institute of Standards and Technology, Gaithersburg, MD, 1995.
- [7] Gritz, L.A., Nicolette, V.F., Moya, J.L., Skocypec, R.D., and Murray, D., "Wind-Induced Interaction of a Large Cylindrical Calorimeter and an Engulfing JP-8 Pool Fire," Proceedings of the Symposium on Thermal Sciences in Honor of Chancellor Chang-Lin Tien, Berkeley, CA, November 14, 1995.
- [8] Budd, L., "F/A-18E/F Engine Nacelle Gas Generator Fire Extinguishing Tests," Naval Air Warfare Center Weapons Division, China Lake, CA, NAWCWPNS TM 7859, March 1995.
- [9] Millsaps, K., *Personal Communication*, Naval Post Graduate School, Monterey, CA.

- [10] Nicolette, V.F., Lopez, A.R., and Gritz, L.A., "F18 Nacelle Fire Simulation," Sandia National Laboratories Technical Memorandum to Leo Budd, January 15, 1997.
- [11] Holen, J., Brostrom, M., and Magnussen, B.F., "Finite Difference Calculation of Pool Fires," 23rd Symposium on Combustion, pp. 1677-1683, 1990.
- [12] Hamins, A., Cleary, T., Borthwick, P., Gorchkov, N., McGrattan, K., Forney, G., Grosshandler, W.L., Presser, C., and Melton, L., "Suppression of Engine Nacelle Fire and Fire Suppression System Performance of Alternative Agents in Aircraft Engine and Dry Bay Laboratory Simulations," NIST Special Publication 890, Vol. II, R.G. Gann, ed., 1995, pp. 1-201.
- [13] Lai, Y.G., Przekwas, A.J., and So, R.M.C., "Aerodynamic Flow Simulation Using a Pressure-Based Method and a Two-Equation Turbulence Model," AIAA Paper No. 93-2902, July 1993.
- [14] Jiang, Y., Lai, Y.G., Ho, S.Y., and Przekwas, A.J., "3D Simulations of Complex Flows with an Implicit Multi-Domain Approach," AIAA Paper No. 93-3124, July 1993.
- [15] Launder, B. E., and Spalding, D. B., "The Numerical Calculation of Turbulent Flows," *Computational Methods Applied to Mechanics and Engineering*, Vol. 3, 1974, pp. 269-289.
- [16] GRIDGEN User's Manual, Version 11, Pointwise, Inc., Bedford, TX, February 1996
- [17] Anderson, J.D., *Modern Compressible Flow*, New York: McGraw-Hill, pp. 49-150, 1982.
- [18] Cussler, E. L., *Diffusion; Mass transfer in fluid systems*, New York: Cambridge University Press, p. 447, 1984.
- [19] Cebeci, T., and Smith, A.M.O., *Analysis of Turbulent Boundary Layers*, New York: Academic Press, pp. 239-240, 1974.
- [20] Beyler, C., "Flammability Limits of Premixed and Diffusion Flames," *Fire Protection Engineering Handbook*, First Edition, Quincy, MA: National Fire Protection Association, Section 1, p. 296, 1988.
- [21] Budd, L., *Personal Communication, Data Acquired during Tests 497 (inboard injection) and 496 (outboard injection)*, Naval Air Warfare Center, Weapons Division, China Lake, CA.
- [22] Magnussen, B.F., "The Eddy Dissipation Concept," Proceedings of the Eleventh Task Leaders Meeting, IEA Working Group on Conservation in Combustion, Lund, Sweden, 1989.
- [23] Tieszen, S.R., Gritz, L.A., and Nicolette, V.F., "FY96 Fire Suppression Progress Report," Sandia National Laboratories Engineering Sciences Research Foundation Internal Report, Sandia National Laboratories, Albuquerque, NM, 1996.